PHOTONICS Research

Increasing the hole energy by grading the alloy composition of the p-type electron blocking layer for very high-performance deep ultraviolet light-emitting diodes

Zi-Hui Zhang,[1,4] Jianquan Kou,[1] Sung-Wen Huang Chen,[2] Hua Shao,[1] Jiamang Che,[1] Chunshuang Chu,[1] Kangkai Tian,[1] Yonghui Zhang,[1] Wengang Bi,[1] and Hao-Chung Kuo[2,3,*]

[1]Institute of Micro-Nano Photoelectron and Electromagnetic Technology Innovation, School of Electronics and Information Engineering, Hebei University of Technology, Key Laboratory of Electronic Materials and Devices of Tianjin, Tianjin 300401, China
[2]Department of Photonics and Institute of Electro-Optical Engineering, Taiwan Chiao Tung University, Hsinchu 30010, China
[3]Department of Electrical Engineering and Computer Sciences and TBSI, University of California at Berkeley, Berkeley, California 94720, USA
[4]e-mail: zh.zhang@hebut.edu.cn
*Corresponding author: hckuo@faculty.nctu.edu.tw

Received 12 December 2018; revised 20 February 2019; accepted 20 February 2019; posted 21 February 2019 (Doc. ID 354950); published 22 March 2019

It is well known that the p-type AlGaN electron blocking layer (p-EBL) can block hole injection for deep ultraviolet light-emitting diodes (DUV LEDs). The polarization induced electric field in the p-EBL for [0001] oriented DUV LEDs makes the holes less mobile and thus further decreases the hole injection capability. Fortunately, enhanced hole injection is doable by making holes lose less energy, and this is enabled by a specifically designed p-EBL structure that has a graded AlN composition. The proposed p-EBL can screen the polarization induced electric field in the p-EBL. As a result, holes will lose less energy after going through the proposed p-EBL, which correspondingly leads to the enhanced hole injection. Thus, an external quantum efficiency of 7.6% for the 275 nm DUV LED structure is obtained.

https://doi.org/10.1364/PRJ.7.0000B1

1. INTRODUCTION

A deep ultraviolet (DUV) light source possesses wide applications in, e.g., air purification, water sterilization, and biosensing. At the current stage, DUV photons are generated by mercury-based fluorescent light emitters. Mercury threatens the health of human organs, such as the nervous system and kidneys. The Minamata Convention on Mercury was initiated in 2017, which requires the elimination of the usage of mercury by the end of 2020 [1]. Therefore, the AlGaN-based DUV light-emitting diode (LED) is emerging as an alternative. One of the very important benchmarks for evaluating DUV LED performance is external quantum efficiency (EQE), which is currently still low [1–4]. The low EQE partly arises from the low hole injection efficiency for DUV LEDs. On one hand, the p-type AlGaN layer has a Mg activation energy from 170 up to 630 meV depending on the AlN composition [5]. The Mg doping efficiency and the corresponding free hole concentration can be remarkably reduced in the Al-rich p-AlGaN layer, i.e., the Mg ionization efficiency can be as low as $\sim 10^{-9}$ [6]. The low Mg doping efficiency further increases the surface depletion width for the p-type contact nitride layer, and this gives rise to the very low hole tunneling efficiency and hinders the hole injection capability [7]. On the other hand, the energy band discontinuity between the p-AlGaN electron blocking layer (p-EBL) and the p-AlGaN layer generates another barrier for hole injection [8]. Note that the AlN composition for the p-EBL is larger than that for the p-AlGaN layer. Accordingly, hole injection can be improved by enhancing the hole tunneling efficiency at the interface of the p-contact/p-type nitride layer, which is doable by optimizing the alloyed metal and/or utilizing the metal/insulator/semiconductor structure [7,9,10]. When the holes arrive at the p-type hole injection layer, hole injection can be improved by enhancing the hole injection, and this can be enabled by adopting the three-dimensional hole gas (3DHG) [11–15]. The hole injection across the p-type hole injection layer can also be promoted, as long as the holes are accelerated such that "hot" holes are generated [8]. The next obstacle for hole transport originates from the p-EBL, and therefore, the valence band barrier height shall be reduced for reducing the hole blocking effect [16–19]. We also report that the [0001] oriented last quantum

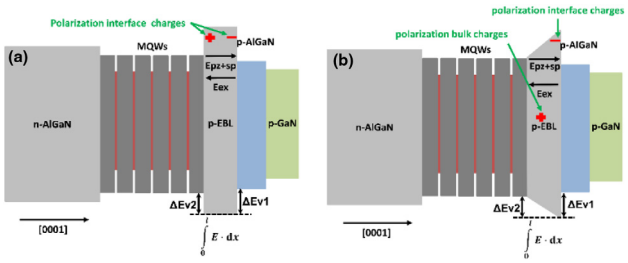

Fig. 1. Schematic energy band diagrams for (a) LED A and (b) LED B. E_{pz+sp} and E_{ex} denote the polarization induced electric field and the electric field that is generated by the external bias, respectively. ΔE_{v1} and ΔE_{v2} present the energy barriers/valence band offsets at the p-EBL/p-AlGaN and the last quantum barrier/p-EBL interfaces, respectively. $\int_0^l E \cdot dx$ reflects the energy that the holes obtain when transporting through the p-EBL. E and l mean the coupled electric field and the thickness for the p-EBL, respectively. Besides the labeled polarization induced interface charges, the polarization induced bulk charges are also symbolized in the p-EBL for LED B.

barrier/p-EBL interface features polarization induced positive charges, which can deplete the holes in the p-EBL. We suggest properly increasing the AlN composition in the AlGaN-based last quantum barrier so that the polarization charge density at the last quantum barrier/p-EBL interface can be decreased, and by doing so, the hole depletion effect in the p-EBL can be suppressed [20]. Meanwhile, the [0001] oriented p-EBL possesses a polarization induced electric field that is opposite to the electric field produced by the external bias, thus decelerating the hole drift velocity, which further hinders hole injection [see Fig. 1(a)]. Therefore, it is very important to screen the polarization induced electric field in the p-EBL and make holes lose less energy.

2. DEVICE STRUCTURES AND PARAMETERS

To achieve that goal, we design and grow two DUV LED structures [LEDs A and B in Figs. 1(a) and 1(b), respectively]. Both structures are grown on a 4 μm thick AlN template, which is deposited on the (0001) planed sapphire substrate. Then, we subsequently grow 20-period $AlN/Al_{0.50}Ga_{0.50}N$ superlattice structures, on which a 2 μm thick n-type $Al_{0.60}Ga_{0.40}N$ layer with the Si doping concentration of 1×10^{18} cm^{-3} is grown. The DUV photons are produced by five-period $Al_{0.45}Ga_{0.55}N/Al_{0.56}Ga_{0.44}N$ multiple quantum wells (MQWs), which produces the peak emission wavelength of 275 nm. The thicknesses for the quantum wells and the quantum barriers are ∼2 nm and ∼12 nm, respectively. Then, two different types of p-EBLs are designed for LEDs A and B. LED A employs a 10 nm thick $Al_{0.60}Ga_{0.40}N$ p-EBL, and the proposed p-EBL that enables the holes to lose less energy is a 40 nm thick $Al_{0.56\rightarrow0.70}Ga_{0.44\rightarrow0.30}N$ p-EBL, such that the AlN composition is linearly increased from 0.56 to 0.70 along the [0001] growth orientation within the 40 nm range. Next, the same p-type hole injection structure comprising the 50 nm p-$Al_{0.40}Ga_{0.60}N$/40 nm p-GaN architecture is grown for the two structures. The hole concentration levels for the p-AlGaN layer and the p-GaN layer are estimated to be 1×10^{17} cm^{-3} and 3×10^{17} cm^{-3}, respectively. Note that we also numerically study LEDs R1 and R2 with a 40 nm thick p-$Al_{0.60}Ga_{0.40}N$ EBL and a 40 nm thick p-$Al_{0.70}Ga_{0.30}N$ EBL, respectively, which can be found in Appendix A.

After the epitaxial growth, flip-chip DUV LED devices are fabricated, and the fabrication processes have been reported in our previous publications [16,21]. The device mesa is fabricated by using inductively coupled plasma etching. We have the mesa size of 650 μm × 320 μm. Ti/Al/Ti/Au is deposited as the n-type ohmic contact, which is then annealed in the N_2 for 1 min at the temperature of 900°C. We use a very thin Ni/Au alloy as the current spreading layer, which is then annealed for 5 min at the temperature of 550°C. Next, we deposit a reflective mirror on the current spreading layer, i.e., Ni/Au/Al/Ti/Au is formed. The electroluminescence is collected from the sapphire side of the DUV LED chip by using an integrating sphere.

To reveal the in-depth origin for the carrier transport, we also conduct numerical calculations by using the advanced physical models of semiconductor devices (APSYS) [2–5,7]. Parameters regarding the non-radiative recombinations include the Shockley–Read–Hall recombination lifetime of 10 ns and Auger recombination coefficient of 1×10^{-30} cm$^6 \cdot$ s^{-1} [22]. The carrier transport is modeled by using the drift-diffusion equations in the non-active layers and the mean-free-path model in the MQW region [23]. The carrier transport in the MQWs is also associated with the energy band offset ratio that is set to 50/50 for AlGaN/AlGaN junctions [24]. We also consider the polarization charge density that is calculated according to Ref. [25], and the polarization level is set to 40%. Specifically, when the p-EBL is compositionally graded for the proposed p-EBL, the polarization induced bulk charges will be generated that can be calculated by referring to the method in Ref. [11]. In our case, the polarization induced bulk charge density is 8.84×10^{17} cm^{-3}. The light extraction efficiency is set to 9% in our models [26].

3. RESULTS AND DISCUSSION

The underlying device physics for LEDs A and B is demonstrated in Figs. 1(a) and 1(b), respectively. For both LEDs A and B, the AlN compositions for the quantum barriers and the p-AlGaN hole injection layer are 0.56 and 0.40, respectively. Therefore, the holes experience a barrier height of ΔE_{v1} when they enter the p-EBL from the p-AlGaN hole injection layer. The arrival of holes at the last quantum barrier after leaving the p-EBL grants the holes with the energy of ΔE_{v2}. Besides, the coupled effect of the polarization induced electric field (E_{pz+sp}) and the external bias induced electric field (E_{ex}) in the p-EBL also affects the energy of the holes, and it can be expressed by $\int_0^l E \cdot dx$, for which E denotes the coupled electric field in the p-EBL, and l represents the thickness for the p-EBL. The net energy (ΔE) that the holes receive during the transport in the p-EBL can be formulated by $\Delta E = \Delta E_{v2} - \Delta E_{v1} + \int_0^l E \cdot dx$. It is known that $\Delta E_{v2} - \Delta E_{v1}$ equals −165.2 meV, meaning that the holes are losing the energy of 165.2 meV. Hence, it is essentially important to "speed up" the holes by using the third term in the equation of ΔE. Note, E_{pz+sp} is opposite to E_{ex} according to Fig. 1(a), and therefore,

the magnitude of the E_{pz+sp} shall be decreased. This is enabled by reducing the polarization effect in the p-EBL, which can be realized by using the polarization self-screening effect [27], such that the polarization induced positive bulk charges in the p-EBL can partially compensate the polarization induced negative interface charges at the p-EBL/p-AlGaN interface. By doing so, the magnitude of E_{pz+sp} can be decreased, which correspondingly makes holes less "cold" and promotes hole injection into the MQWs.

To probe the effectiveness of the proposed p-EBL in improving the hole injection and the EQE for DUV LEDs, we measure and present the relationship between the current density and the applied bias in Fig. 2(a), which shows that the forward operation voltage for LED B decreases when compared with LED A. Figure 2(b) presents the measured EQE and the optical power density for our devices, and we can see that a very high EQE of 7.6% is produced by LED B, which translates to an EQE enhancement of 1.5 times. Moreover, we numerically reproduce the experimentally measured optical power density in Fig. 2(b). By using the low-temperature photoluminescence method, the internal quantum efficiency (IQE) is measured to be ~60% for LED B, and the calculated IQE is ~65% by using our models. As a result, the excellent agreement between the measured and the calculated results further indicates that the employed models are convincing for our devices. Figure 2(c) shows the normalized electroluminescent (EL) spectra for LEDs A and B, and the peak emission wavelength for the two devices is ~275 nm. The parasitic emission wavelength of 425 nm is found in the p-type hole injection layers. Nevertheless, the parasitic emission intensity for LED B is lower than that for LED A, which is likely due to the suppressed electron leakage for LED B with the proposed p-EBL.

To reveal the origin for the observations in Figs. 2(a)–2(c), we calculate the hole concentration in Fig. 3(a), which demonstrates that the hole concentration in the MQWs for LED B increases when compared to that for LED A. Figure 3(b) shows the electron concentration profiles in the p-type hole injection layer, and we can see that the leakage electrons for LED B have been significantly decreased. The reduced concentration for the leakage electrons in the p-type hole injection layers suppresses the parasitic recombination between the electrons and the holes

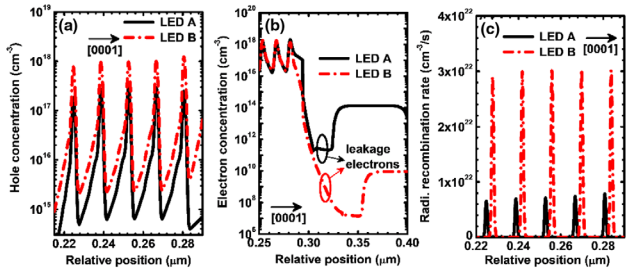

Fig. 3. Numerically computed (a) hole concentration profiles in the MQWs, (b) electron concentration profiles in the last three quantum wells and the p-type hole injection layers, and (c) radiative recombination rate profiles in the MQWs for LEDs A and B, respectively. The data are calculated at the current density of 50 A/cm^2. Calculated hole concentration, electron concentration, and radiative recombination rate for LEDs R1 and R2 with the 40 nm thick p-$Al_{0.60}Ga_{0.40}N$ EBL and the 40 nm thick p-$Al_{0.70}Ga_{0.30}N$ EBL, respectively, can be found in Appendix A.

therein, and this interprets the smaller parasitic emission intensity for LED B in Fig. 2(c). The numerically computed radiative recombination rate profiles in the MQWs for LEDs A and B are shown in Fig. 3(c), which illustrates that the radiative recombination rate for LED B has been remarkably improved. The substantially promoted radiative recombination rate for LED B is well ascribed to the enhanced hole injection efficiency [see Fig. 3(a)]. Moreover, the improved hole injection and the enhanced radiative recombination rate in the MQWs help to generate more electrical current, thus reducing the forward operation voltage for LED B according to Fig. 2(a).

Lastly, in order to show the in-depth origin for the enhanced hole concentration in the MQWs and the suppressed electron leakage level in the p-type hole injection layers for LED B, we show the energy band profiles of the p-EBL and the p-type hole injection layers for LEDs A and B in Figs. 4(a) and 4(b), respectively. Here, we define the effective barrier height for carriers, i.e., the energy difference between the quasi-Fermi level for electrons/holes and the conduction band/valence band, which are shown as ϕ_e and ϕ_h in Figs. 4(a) and 4(b). The effective energy band barrier height here is different from the previously defined energy barrier [i.e., ΔE_{v1} and ΔE_{v2} in

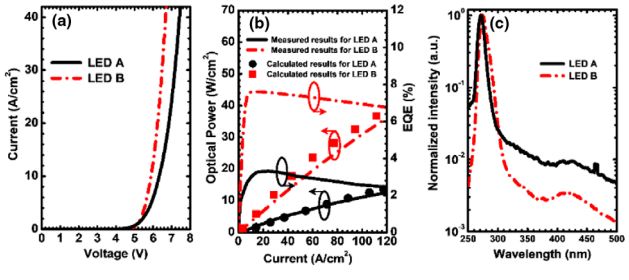

Fig. 2. (a) Measured current–voltage characteristics, (b) measured EQE and optical power density in terms of the injection current, where the optical power density is also numerically calculated, and (c) measured EL spectra with the intensity normalized to one for LEDs A and B. Calculated optical power for LEDs R1 and R2 with the 40 nm thick p-$Al_{0.60}Ga_{0.40}N$ EBL and the 40 nm thick p-$Al_{0.70}Ga_{0.30}N$ EBL, respectively, can be found in Appendix A.

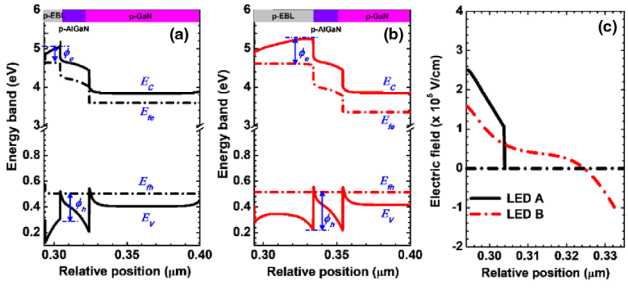

Fig. 4. Calculated energy band profiles of the p-EBLs and the p-type hole injection layers for (a) LED A and (b) LED B, and (c) calculated electric field profiles in the p-EBLs for LEDs A and B. The data are calculated at the current density of 50 A/cm^2. Calculated energy bands for LEDs R1 and R2 with the 40 nm thick p-$Al_{0.60}Ga_{0.40}N$ EBL and the 40 nm thick p-$Al_{0.70}Ga_{0.30}N$ EBL, respectively, can be found in Appendix A.

Fig. 1]. Figures 4(a) and 4(b) show that the values of ϕ_e of the p-EBLs are 386 and 682 meV for LEDs A and B, respectively. The larger ϕ_e for the proposed p-EBL well explains the reduced electron leakage level for LED B, as shown in Fig. 3(b). The increased ϕ_e for the proposed p-EBL originates from the improved hole concentration level across the MQWs for LED B, which enables the formation of more electron–hole pairs for the better radiative recombination [see Fig. 3(c)]. Correspondingly, the electrons will be less accumulated in the last quantum barrier, which helps to pull the quasi-Fermi level for electrons apart from the conduction band, thus increasing the effective conduction band barrier height for the proposed p-EBL [27].

Surprisingly, when we look at Figs. 4(a) and 4(b), we can find that the effective valence band barrier height of ϕ_h for LED B is larger than that for LED A, i.e., the values of ϕ_h for the two different p-EBLs are 200 and 300 meV, respectively. Therefore, by merely using ϕ_h, the enhanced hole concentration level in the MQWs for LED B cannot be understood. Therefore, we further calculate and present the electric field profiles in the p-EBLs for LEDs A and B in Fig. 4(a), which shows that the polarization self-screening effect reduces the electric field intensity in the proposed p-EBL for LED B [27]. The mesh distributions for the p-EBLs have been properly optimized, and, by using the equation of $\int_0^l E \cdot dx$, we are able to get the integration values of 169.12 and 128.87 meV for LEDs A and B, respectively. Therefore, the polarization induced electric field in the proposed p-EBL for LED B can decelerate the hole transport less. By combining the aforementioned ΔE of $\Delta E_{v2} - \Delta E_{v1}$ that is 165.2 meV for both LEDs, during the hole transport from the p-EBL/p-AlGaN interface to the last quantum barrier/p-EBL interface, the energy loss of the holes is 334.32 and 294.07 meV for LEDs A and B, respectively. Therefore, the holes for LED B are less decelerated than the holes for LED A. Hence, those holes that climb over the barrier of ϕ_h can be more effectively injected into the MQWs, and we believe the hole injection capability can be further promoted if the effective valence band barrier height of the p-EBL for LED B can be reduced more.

4. CONCLUSIONS

To summarize, this work has proposed a p-EBL with the graded AlN composition to improve the DUV LED performance. The EQE and the optical power density for the DUV LED with the proposed p-EBL have been significantly boosted by 1.5 times. The experimental observations are further verified by numerical calculations. We find that the proposed p-EBL enables highly efficient hole injection, and suppressed electron leakage is simultaneously obtained. The enhanced hole injection is attributed to the fact that the polarization self-screened feature for the proposed p-EBL screens the polarization induced electric field, and as a result, the holes will be made less decelerated after traveling through the proposed p-EBL. The enhanced hole concentration in the MQW region favors the very pronounced radiative recombination rate. The hole drift current and the current that is caused by the radiative recombination in the MQWs account for the reduced forward voltage for the proposed DUV LED. Our findings indicate that the EQE and the optical power density can be even further promoted once the valence band barrier height for the proposed p-EBL is reduced, e.g., a composition-graded junction is adopted for the p-EBL/p-AlGaN architecture. We believe the proposed approach and the reported device physics in this work are very useful for the DUV LED community.

APPENDIX A

In order to probe the impact of the thickness and the Al composition of the p-EBL on the emission properties for DUV LEDs, we further study LEDs R1 and R2. The device architectures for LEDs R1 and R2 are identical to LEDs A and B except for the p-EBL. LEDs R1 and R2 employ a 40 nm thick p-$Al_{0.60}Ga_{0.40}N$ EBL and a 40 nm thick p-$Al_{0.70}Ga_{0.30}N$ EBL, respectively.

We numerically calculate the optical power density in terms of the injection current density for the four investigated DUV LEDs [see Fig. 5]. We can see that when the thickness for the p-EBL increases, the optical power density increases. Further comparison between LEDs R1 and R2 indicates that the p-$Al_{0.70}Ga_{0.30}N$ EBL degrades the optical power density. Nevertheless, LED B generates the strongest optical power density among the studied devices.

We then calculate and show the hole concentration profiles, the electron concentration profiles, and the radiative recombination rates for LEDs A, B, R1, and R2 in Figs. 6(a), 6(b), and 6(c), respectively. Figure 6(a) presents that the hole concentration levels in the MQW regions for LEDs R1 and R2 increase when compared to LED A. LED B shows the highest hole concentration level in the active region. Figure 6(b) demonstrates the electron leakage level for the four devices. We can see that, for the current device architectures, making the p-EBL thick and/or increasing the Al composition for the p-EBL does not reduce the electron leakage according to the comparison among LEDs A, R1, and R2. Figure 6(c) shows the radiative recombination rate profiles across the MQW regions for the four DUV LEDs. We can get the lowest radiative recombination rate from LED A. The improved hole concentration enhances the radiative recombination rate for LEDs R1 and R2. LED B yields the strongest radiative recombination rate. Figure 6(c) agrees well with Fig. 5.

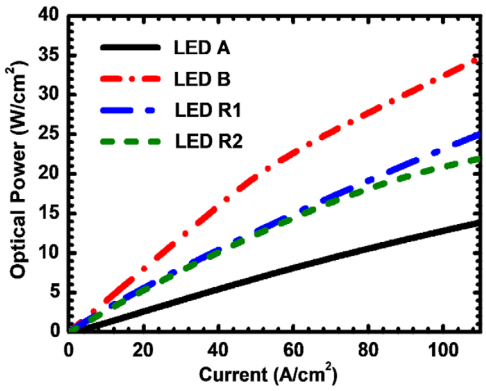

Fig. 5. Numerically calculated optical power density for LEDs A, B, R1, and R2. LEDs R1 and R2 have a 40 nm thick p-$Al_{0.60}Ga_{0.40}N$ EBL and a 40 nm thick p-$Al_{0.70}Ga_{0.30}N$ EBL, respectively.

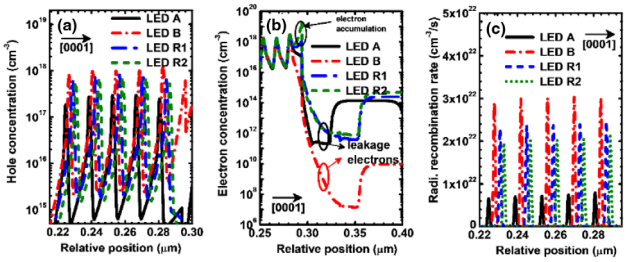

Fig. 6. Numerically calculated (a) hole concentration profiles in the MQWs, (b) electron concentration profiles in the MQWs and the p-type layers, and (c) radiative recombination rate across the MQW region for LEDs A, B, R1, and R2. For better resolution, the position for the hole concentration and the radiative recombination rate of LEDs B, R1, and R2 are purposely shifted by 0.002, 0.004, and 0.006 μm with reference to LED A. The data are calculated at the current density of 50 A/cm^2.

To interpret Figs. 6(a) and 6(b) at an in-depth level, we calculate and show the energy band diagrams of the p-EBLs for LEDs A, B, R1, and R2 in Figs. 7(a), 7(b), 7(c), and 7(d), respectively. We can see that the energy bands of the last quantum barriers for LEDs R1 and R2 are both bent upwards, such that the energy level for point A is higher than that for point B, which favors the hole transport. On the contrary, the energy level for point A is lower than that for point B for LEDs A and B, which retards the hole injection. As a result, the hole concentrations in the MQWs for LEDs R1 and R2 are larger than that for LED A. The even better hole injection for LED R1 than that for LED R2 arises from the smaller blocking effect by the p-$Al_{0.60}Ga_{0.40}N$ EBL. It is worth noting that, although the hole blocking effect is encountered in the last quantum barrier, the hole concentration level is most promoted for LED B, and such interesting observations have been explained in detail in the main text for this work.

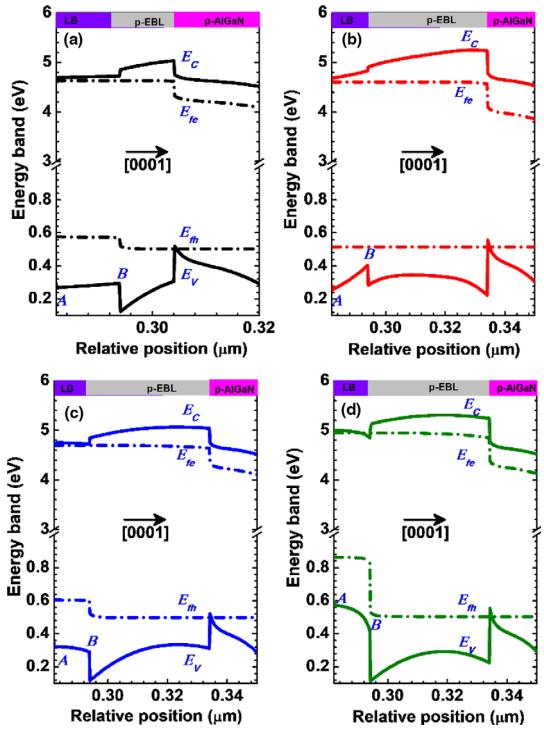

Fig. 7. Calculated energy band profiles of the p-EBLs and the p-type hole injection layers for (a) LED A, (b) LED B, (c) LED R1, and (d) LED R2. E_C, E_V, E_{fe}, and E_{fh} denote the conduction band, the valence band, and the quasi-Fermi levels for electrons and holes, respectively. The data are calculated at the current density of 50 A/cm^2.

The last quantum barriers for Figs. 7(c) and 7(d) indicate that the conduction band is closely approaching the quasi-Fermi level, which means that electron accumulation occurs at the last quantum barrier/p-EBL interface [see Fig. 6(b)]. The very strong electron accumulation at the last quantum barrier/p-EBL interface causes significant electron leakage for LEDs R1 and R2 [27,28]. Therefore, without specific design, it is of less contribution in suppressing the electron leakage merely by increasing the thickness or/and the Al composition for the p-EBL.

Funding. National Natural Science Foundation of China (NSFC) (51502074); Natural Science Foundation of Hebei Province (F2017202052); Natural Science Foundation of Tianjin City (16JCYBJC16200); Program for Top 100 Innovative Talents in Colleges and Universities of Hebei Province (SLRC2017032); Program for 100-Talent-Plan of Hebei Province (E2016100010).

Acknowledgment. The authors of this work acknowledge TESS Corporation in Korea, Epistar Corp. in China, and Prof. Hideto Miyake of Mie University.

REFERENCES

1. Y. Nagasawa and A. Hirano, "A review of AlGaN-based deep-ultraviolet light-emitting diodes on sapphire," Appl. Sci. **8**, 1264 (2018).
2. D. B. Li, K. Jiang, X. J. Sun, and C. L. Guo, "AlGaN photonics: recent advances in materials and ultraviolet devices," Adv. Opt. Photon. **10**, 43–110 (2018).
3. A. Khan, K. Balakrishnan, and T. Katona, "Ultraviolet light-emitting diodes based on group three nitrides," Nat. Photonics **2**, 77–84 (2008).
4. H. Hirayama, N. Maeda, S. Fujikawa, S. Toyoda, and N. Kamata, "Recent progress and future prospects of AlGaN-based high-efficiency deep-ultraviolet light-emitting diodes," Jpn. J. Appl. Phys. **53**, 100209 (2014).
5. Y.-H. Liang and E. Towe, "Progress in efficient doping of high aluminum-containing group III-nitrides," Appl. Phys. Rev. **5**, 011107 (2018).
6. K. B. Nam, M. L. Nakarmi, J. Li, J. Y. Lin, and H. X. Jiang, "Mg acceptor level in AlN probed by deep ultraviolet photoluminescence," Appl. Phys. Lett. **83**, 878–880 (2003).
7. Z.-H. Zhang, Y. Zhang, W. Bi, C. Geng, S. Xu, H. V. Demir, and X. W. Sun, "A charge inverter for III-nitride light-emitting diodes," Appl. Phys. Lett. **108**, 133502 (2016).
8. Z.-H. Zhang, L. Li, Y. Zhang, F. Xu, Q. Shi, B. Shen, and W. Bi, "On the electric-field reservoir for III-nitride based deep ultraviolet light-emitting diodes," Opt. Express **25**, 16550–16559 (2017).
9. K. H. Kim, T. H. Lee, K. R. Son, and T. G. Kim, "Performance improvements in AlGaN-based ultraviolet light-emitting diodes due to electrical doping effects," Mater. Des. **153**, 94–103 (2018).
10. H. K. Kim, T. Y. Seong, I. Adesida, C. W. Tang, and K. M. Lau, "Low-resistance Pt/Pd/Au ohmic contacts to p-type AlGaN," Appl. Phys. Lett. **84**, 1710–1712 (2004).
11. J. Simon, V. Protasenko, C. Lian, H. Xing, and D. Jena, "Polarization-induced hole doping in wide-band-gap uniaxial semiconductor heterostructures," Science **327**, 60–64 (2010).

12. L. Zhang, K. Ding, J. C. Yan, J. X. Wang, Y. P. Zeng, T. B. Wei, Y. Y. Li, B. J. Sun, R. F. Duan, and J. M. Li, "Three-dimensional hole gas induced by polarization in (0001)-oriented metal-face III-nitride structure," Appl. Phys. Lett. **97**, 062103 (2010).
13. S. Li, M. Ware, J. Wu, P. Minor, Z. Wang, Z. Wu, Y. Jiang, and G. J. Salamo, "Polarization induced pn-junction without dopant in graded AlGaN coherently strained on GaN," Appl. Phys. Lett. **101**, 122103 (2012).
14. Y. Zhang, S. Krishnamoorthy, F. Akyol, A. A. Allerman, M. W. Moseley, A. M. Armstrong, and S. Rajan, "Design of p-type cladding layers for tunnel-injected UVA light emitting diodes," Appl. Phys. Lett. **109**, 191105 (2016).
15. J. Verma, S. M. Islam, V. Protasenko, P. K. Kandaswamy, H. Xing, and D. Jena, "Tunnel-injection quantum dot deep-ultraviolet light-emitting diodes with polarization-induced doping in III-nitride heterostructures," Appl. Phys. Lett. **104**, 021105 (2014).
16. Z.-H. Zhang, S.-W. H. Chen, Y. Zhang, L. Li, S.-W. Wang, K. Tian, C. Chu, M. Fang, H.-C. Kuo, and W. Bi, "Hole transport manipulation to improve the hole injection for deep ultraviolet light-emitting diodes," ACS Photon. **4**, 1846–1850 (2017).
17. M. M. Satter, Z. Lochner, T.-T. Kao, Y.-S. Liu, X.-H. Li, S.-C. Shen, R. D. Dupuis, and P. D. Yoder, "AlGaN-based vertical injection laser diodes using inverse tapered p-waveguide for efficient hole transport," IEEE J. Quantum Electron. **50**, 166–173 (2014).
18. Y.-S. Liu, T.-T. Kao, M. M. Satter, Z. Lochner, S.-C. Shen, T. Detchprohm, P. D. Yoder, R. D. Dupuis, J.-H. Ryou, A. M. Fischer, and Y. O. Wei, "Inverse-tapered p-waveguide for vertical hole transport in high-[Al] AlGaN emitters," IEEE Photon. Technol. Lett. **27**, 1768–1771 (2015).
19. L. Lu, G. G. Ding, Y. Zhang, and F. J. Xu, "Improved performance of AlGaN-based deep ultraviolet light-emitting diode using modulated-taper design for p-AlGaN layer," Semicond. Sci. Technol. **33**, 035008 (2018).
20. Z.-H. Zhang, C. Chu, C. H. Chiu, T. C. Lu, L. Li, Y. Zhang, K. Tian, M. Fang, Q. Sun, H.-C. Kuo, and W. Bi, "UVA light-emitting diode grown on Si substrate with enhanced electron and hole injections," Opt. Lett. **42**, 4533–4536 (2017).
21. Z.-H. Zhang, S.-W. H. Chen, C. Chu, K. Tian, M. Fang, Y. Zhang, W. Bi, and H.-C. Kuo, "Nearly efficiency-droop-free algan-based ultraviolet light-emitting diodes with a specifically designed superlattice p-type electron blocking layer for high Mg doping efficiency," Nanoscale Res. Lett. **13**, 122 (2018).
22. Y.-K. Kuo, J.-Y. Chang, F.-M. Chen, Y.-H. Shih, and H.-T. Chang, "Numerical investigation on the carrier transport characteristics of AlGaN Deep-UV light-emitting diodes," IEEE J. Quantum Electron. **52**, 3300105 (2016).
23. Z.-H. Zhang, W. Liu, S. T. Tan, Z. Ju, Y. Ji, Z. Kyaw, X. Zhang, N. Hasanov, B. Zhu, S. Lu, Y. Zhang, X. W. Sun, and H. V. Demir, "On the mechanisms of InGaN electron cooler in InGaN/GaN light-emitting diodes," Opt. Express **22**, A779–A789 (2014).
24. J. Piprek, "Efficiency droop in nitride-based light-emitting diodes," Phys. Status Solidi A **207**, 2217–2225 (2010).
25. V. Fiorentini, F. Bernardini, and O. Ambacher, "Evidence for nonlinear macroscopic polarization in III–V nitride alloy heterostructures," Appl. Phys. Lett. **80**, 1204–1206 (2002).
26. H.-Y. Ryu, I.-G. Choi, H.-S. Choi, and J.-I. Shim, "Investigation of light extraction efficiency in AlGaN deep-ultraviolet light-emitting diodes," Appl. Phys. Express **6**, 062101 (2013).
27. Z.-H. Zhang, W. Liu, Z. Ju, S. T. Tan, Y. Ji, X. Zhang, L. Wang, Z. Kyaw, X. W. Sun, and H. V. Demir, "Polarization self-screening in [0001] oriented InGaN/GaN light-emitting diodes for improving the electron injection efficiency," Appl. Phys. Lett. **104**, 251108 (2014).
28. Z.-H. Zhang, Y. Zhang, H. Li, S. Xu, C. Geng, and W. Bi, "On the importance of the polarity for GaN/InGaN last quantum barriers in III-nitride-based light-emitting diodes," IEEE Photon. J. **8**, 8200307 (2016).